Electrochimica Acta 163 (2015) 323–329

Contents lists available at ScienceDirect

Electrochimica Acta

journal homepage: www.elsevier.com/locate/electacta

$LiFePO_4$ particle conductive composite strategies for improving cathode rate capability

Nuria Vicente [a], Marta Haro [a], Daniel Cíntora-Juárez [b], Carlos Pérez-Vicente [b], José Luis Tirado [b], Shahzada Ahmad [c,*], Germà Garcia-Belmonte [a,*]

[a] Photovoltaics and Optoelectronic Devices Group, Departament de Física, Universitat Jaume I, 12071 Castelló, Spain
[b] Laboratorio de Química Inorgánica, Campus de Rabanales, Universidad de Córdoba, 14071, Spain
[c] Abengoa Research, Abengoa, C/Energía Solar n° 1, Campus Palmas Altas, 41014 Seville, Spain

ARTICLE INFO

Article history:
Received 14 January 2015
Received in revised form 17 February 2015
Accepted 17 February 2015
Available online 18 February 2015

Keywords:
$LiFePO_4$ composite
impedance spectroscopy
conductive polymer

ABSTRACT

Lithium iron phosphate (LFP) cathodes are one of the most promising candidates to find application in hybrid electric vehicle energy storage system. For this reason advances in the performance of its theoretical capacity at high charge/discharge rates is under continuous development. Most used strategies to improve power performance are the addition to the LFP particles of an electric conductive carbon or polymer, such as poly(3,4-ethylenedioxythiophene) [PEDOT] doped with polystyrene sulfonate (PSS). The data obtained from impedance analysis provide new insight on the role of these additives that not only improve the charge transfer but also favor the lithiation/delithiation processes in the phosphate matrix. Furthermore, PEDOT is capable to reduce the resistances of charge transfer and lithiation reaction inside the phosphate matrix by one order of magnitude in comparison with those achieved with the carbon coating strategy. In this study, the most effective approach has been the addition of PEDOT by a blending method, resulting in a specific capacity of 130 mA h g_{LFP}^{-1} at 2 C.

1. Introduction

In the last decades, lithium iron phosphate ($LiFePO_4$) has been extensively studied, and currently it is regarded as one of the most likely candidate for the large-sized Li-ion batteries for hybrid electric vehicles (HEV) [1]. Other applications include cathode in portable electronic devices, bulk electricity storage at power stations and to provide back-up energy for solar and wind power [2,3]. This electrode has attracted extensive attention due to a high theoretical specific capacity (170 mAh g^{-1}), high stability, low cost, high compatibility with environment, and small amount of oxygen generation at the fully charged state. Its main drawback is to attain the full capacity due to its low electronic conductivity which leads to initial capacity loss and poor rate capability.

To gain the full capacity of these materials, the mechanism of charging–discharging of this cathode has been deeply studied [4,5] and explained in terms of charge transfer followed by a phase change, denominated "domino-cascade model" [4]. In the $LiFePO_4$ olivine structure, the oxygen atoms adopt a hexagonal closed-packing configuration with Li^+ and Fe^{2+} cations located in half of the octahedral sites and P^{5+} cations in 1/8 of tetrahedral sites. Then, there exist 1D channels for Li^+ ions exchange. Once the mechanism is understood, several strategies have been investigated to improve both electronic and ionic conductivity to overcome the current bottleneck in these materials. Two of these strategies are the addition to the LFP particles of electric conductive carbon and/or polymers. Carbon improves the electronic conductivity and can contribute to increase the electrode capacity [6–10]. However, perfect surface coatings and desired mixtures are often very difficult to achieve and the power-performance enhancement of these electrode materials is still limited. More recently, the use of conductive polymers such as poly(3,4-ethylenedioxythiophene) (PEDOT) doped with polystyrene sulfonate (PSS) is especially attractive in terms of the improvement of the mechanical flexibility, the option to be coated under mild processing conditions compared to carbon coating, improvement of Li-ion transport, and for its dual role as conductive and binder additive [11–13]. For these reasons, PEDOT like other materials such as ZnO, [14] has increased interest in the energy scientific community with multipurpose features and applications (photovoltaics, photo-electrochemistry besides in energy storage) [15]. In these cathodes,

* Corresponding author.
E-mail address: garciag@uji.es (G. Garcia-Belmonte).

http://dx.doi.org/10.1016/j.electacta.2015.02.148
0013-4686/

the synthesis procedure is the key for the final stoichiometry and microsctructure that largely influence the physico-chemical properties of the material.

LFP can be directly prepared by ceramic procedures. Normally, solid precursor compounds such as Fe(II)-acetate, ammonium phosphate and lithium carbonate are mixed together in a ball mill, and a first mild temperature treatment is used to achieve their decomposition [16]. The final thermal treatment up to 900 °C is carried out in an inert or slightly reducing atmosphere to avoid Fe^{2+} to Fe^{3+} oxidation. The addition of carbon sources such as citric acid is also used for this purpose. With sufficient carbon excess, e.g. by covering the pellets with carbon black, the resulting LFP particles are carbon-coated and display improved conductive properties [17]. Due care must be taken to avoid an extended formation of iron phosphide that may penalize the capacity, although being also a conductive side product [18]. To lower the reaction temperature, LFP can also be synthesized by solvothermal methods. The hydrothermal procedure starting from $FeSO_4{\cdot}7H_2O$ and o-H_3PO_4 premixed with water by addition of a LiOH solution [19] can be carried out in both subcritic and supercritic conditions, the later favoring a higher dispersion of the resulting powders. Ionothermal [20], polyol [18], non-aqueous sol–gel syntheses [21] and coprecipitation in aqueous medium [22] have also been successfully employed.

Recently, we have proposed a model to study the lithiation/delithiation kinetics through equivalent circuit analysis of the experimentally obtained electrochemical impedance spectroscopy (EIS) spectra [23,24]. This approach facilitates the extraction of resistances involved in the overall lithium ion storage that allows establishing mechanisms for rate capability reduction, as well as the insertion–extraction process occurring during the battery cycling. Herein, $LiFePO_4$ (LFP) composites were prepared with PEDOT:PSS to give molecular wiring effect (LFP/PEDOT), carbon (C-LFP), and both materials (C-LFP/PEDOT). The role of each element has been analyzed by impedance spectroscopy that can distinguish the different steps involved in the charge–discharge process associated to the specific electrochemical mechanisms and, by means of a proposed equivalent circuit model, the different processes can be related to resistances and capacitances. The obtained data show that PEDOT reduces the resistances of charge transfer and lithiation reaction by one order of magnitude respect to those extracted employing carbon coatings, which gives a new resistance and capacity ascribed to the carbon film. Albeit the lithiation/delithiation mechanism has been extensively studied in olivine cathodes, novel insight into the electrical contributions of each element is obtained through the resistive analysis of the recorded impedance spectra.

2. Experimental

LFP was obtained as described elsewhere [25]. For C-coating, samples were pressed into pellets that were then covered with excess carbon black ca. 1 g/400 mg of sample and then heated in alumina boats at 750, 850, and 900 °C for 8 and 16 h. Then, the remaining carbon black excess was mechanically removed. Electrodes were also prepared by mixing the LFP or LFP/C active materials with CB and PVDF (85:8:7 wt.) in *N*-methyl pyrrolidone. The mixture was sonicated and deposited over aluminum disks (0.64 cm^2). Finally, the deposits were dried at 80 °C under vacuum for 12 h. The average amount of LFP in the electrodes is estimated at 5 mg cm^{-2}. Samples with PEDOT:PSS where obtained by two methods. The first method (blend) consisted in mixing PEDOT:PSS (0.3 mg) with LFP, PVDF and CB. For the second method (dropcast), PEDOT:PSS (0.3 mg) was casted over a preformed LFP or C-LFP electrode. For both methods, the electrodes were dried under vacuum at 100 °C for 12 h.

Scanning electron microscopy (SEM) images were obtained using a JEOL JSM63000 microscope. The electrochemical characterization was carried out using a two-electrode Swagelok cell with metallic lithium as both the counter and the reference electrode, and a glass fiber (Grade GF/C260 μm-thick) from Whatman as a separator. The electrolyte used was 1.0 M $LiPF_6$ in a 50:50 (w/w) mixture of ethylene carbonate (EC) and diethyl carbonate (DEC). Cell assembly was carried out in a N_2-filled glovebox. Electrochemical characterization was performed using a PGSTAT-30 potentiostat from Autolab equipped with an impedance module. 1 C was defined as 170 mA g_{LFP}^{-1} for the charge–discharge tests. The cyclic voltammetry (CV) and the galvanostatic charge/discharge tests were carried out in the voltage window of 2–4.5 V. After three CV scans, the EIS spectra were measured (every 200 mV) within this voltage range with amplitude of 10 mV, in the frequency range of 1 MHz to 1 mHz. The EIS spectra were registered first in the discharge direction and later in the charge direction. The approximation to the different voltages of measurement was potentiostically controlled at 10 μV s^{-1} to assure the quasi-equilibrium state of the battery. Also, before each measurement the system was stabilized during 30 minutes.

The experimental data are normalized to the mass of LFP, although the masses of PEDOT and C are the same in the electrodes, and the relationship of the values maintain the same trend if it was referred to the mass of the electrode.

3. Results and discussion

3.1. Characterization of LFP based electrodes

Fig. 1a shows particles of pristine LFP, while Fig. 1b shows the LFP coated with PEDOT:PSS. It can be observed that the virgin LFP is of irregular shape while the modified LFP cathode with PEDOT:PSS has uniformly covered the surface resembling a blanket coating atop of LFP. The granular structures of LFP are in close contact with PEDOT resulting in a material with enhanced mechanical and electrical connection between the active particles.

3.2. Electrochemical response

Fig. 2 shows the 3rd cycle of the cyclic voltammetry signal of the LFP-based cathodes, where the Fe^{3+}/Fe^{2+} redox reaction peaks upon lithium intercalation are observed within the range of 2–4.5 V. The faradaic processes related to the Li^+ ion insertion and extraction from the LFP lattice are clearly favored in the cathode LFP/PEDOT(blend), which shows the closest and narrowest peaks, followed by LFP/PEDOT(cast) electrode that shows similar behavior to C-LFP/PEDOT(cast) cathode. The C-LFP electrodes (without PEDOT) show the Li^+ ion insertion and extraction peaks with a separation of almost 2 V. The width of the peaks and the separation between them are related to the kinetic limitations (resistances) present in the electrode. Besides residual hysteresis unveiled in multiparticulate LFP electrodes at extremely low currents was ascribed to thermodynamic phenomena in a recent study [25]. According to the CV experiments, PEDOT reduces the resistances in the system, in particular for the blend preparation, while the effect of C-coating is considerably less significant.

The third cycle of the charge–discharge curves obtained at different rates for the LFP/PEDOT, C-LFP/PEDOT, and C-LFP electrodes are shown in Fig. 3a–d. In all cases, as the current density increases, the charge–discharge plot shows that the specific capacity decreases, which indicates low active material utilization and transport limitations in the solid $LiFePO_4$ particles [26]. This effect is clearly observed in Fig. 3e that shows the effect of the cycle number and the charging–discharging rate on the capacity of the cathode. At very low current, C/10, the discharge

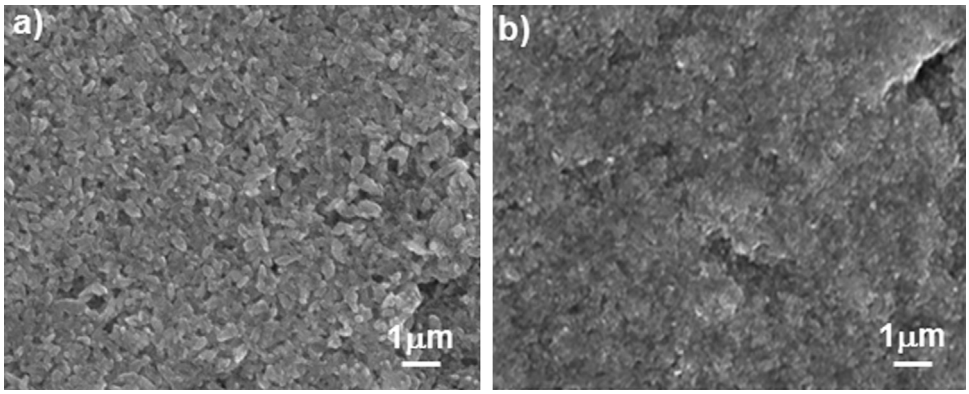

Fig. 1. Scanning electron microscopy images of a) pristine LFP and b) LFP/PEDOT electrodes.

specific capacity is similar for all the studied electrodes, with slightly larger values for C-LFP-PEDOT(cast) and lower for LFP-PEDOT(cast). As the discharge current increases the battery with higher specific capacity is LFP-PEDOT(blend) that provides 130 mA h g_{LFP}^{-1} at 2 C. Meanwhile, when the polymer is drop cast over LFP and C-LFP, the specific capacity collapses at C and 2 C rates, respectively. After such tests, these last electrodes show no response even at low charge current (C/10). This phenomenon suggests that the lost of capacity is related to stability issues rather than kinetic barriers. This elucidation was also supported by the CV experiments, in which both electrodes show better defined redox peaks than the C-LFP sample, which suggests lower resistance values. The kinetic limitations are clearly observed for C-LFP that shows similar specific capacity than LFP-PEDOT-blend at low discharge current (C/10, C/5), however it decreases notably above C/2, reaching a value of 50 mAh g_{LFP}^{-1} at 2 C (less than half the value obtained for LFP-PEDOT(blend)).

The other feature observed in Fig. 3a–d is reflected in Fig. 3f. As the current density increases the mid plateau potential decreases (increases), and the voltage gap resulting from the hysteresis increases. This effect has been assigned to a combination of transport and ohmic losses with negligible contribution from the kinetics of the charge-transfer reaction [26]. The lowest hysteresis is for the sample LFP/PEDOT(blend) that scarcely increases with the charge–discharge rate. The small value of the gap at moderate 1 C rate suggests that blended PEDOT favors the transport of both Li^+ ions and e^- within the LFP bulk. It is evident that the electrode preparation method is critical for the battery operation. Thus, when the PEDOT is cast in the cathode, the transport and ohmic losses increases dramatically. On the other hand, the C coverage reduces these losses to some extent.

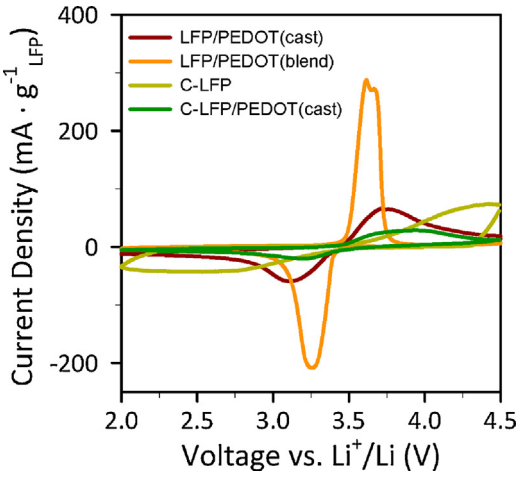

Fig. 2. Cyclic voltammograms of LFP composites with C and/or PEDOT at 0.1 mV·s^{-1}.

In summary, coating with a conductive polymer such as PEDOT reduces the transport limitations in the solid $LiFePO_4$ particles and increases the rate performance of the cathode. The carbon coating improves thermodynamic properties, while the kinetic behavior is more restricted in comparison with PEDOT coatings. Further to distinguish the effect of PEDOT and C in the cathodes, the impedance spectra of fabricated batteries are discussed in the next section by means of EIS technique. The samples prepared with PEDOT (cast) show worse electrical response than those using blend method and have lower stability, thus the impedance spectra is discussed in the Supplementary Information (SI). It is noteworthy that synthesis method is crucial in the cathode operation and the following discussion is valid for the particular PEDOT and C deposition in LFP cathodes described in this manuscript.

3.3. Electrochemical impedance spectroscopy analysis

Aiming at uncovering the origin for the superior rate capability exhibited by LFP/PEDOT(blend) cathodes, the assembled half batteries were characterized by means of EIS to discern the different steps involved in the charge–discharge process. Minor contributions are expected from the Li counterelectrode assimilated to the series resistance. After three CV cycles, the EIS measurements were carried out potentiostatically at different stages of the Li^+ ion insertion and extraction at a very low rate to ensure the steady-state condition. Fig. 4 shows, as example, different Nyquist diagrams experimentally obtained during the lithiation process. The Nyquist plots for the delithiation process are represented in the SI, where the discussion is similar to that reported in the text for the lithiation process.

In general terms, the impedance spectra exhibit two patterns with distinguishable time constants associated to specific electrochemical mechanisms and an additional series resistance that accounts for the solution contribution, $R_s \approx 9\,\Omega$. First, at high frequencies a flattened arc is observed related to the interfacial charge transfer resistance, R_{ct}, in parallel with the double layer capacitance, C_{dl}. A detail of this arc shows in the case of C-LFP an additional small arc (effect clearly observed in the representation of capacitances that is shown and discussed in SI) related to the resistance and capacitance of the C-coating, R_C and C_C. Second, at low frequencies, the Nyquist plots show a capacitive behavior associated with the Li^+ ion storage inside the cathode which is manifested by its chemical capacitance, C_μ. [27] This capacitance refers to the differential change in electrode charge upon voltage variation and it is connected to the ability of the phosphate matrix to intercalate Li^+ ions. In fact it is a quasi-equilibrium (extremely

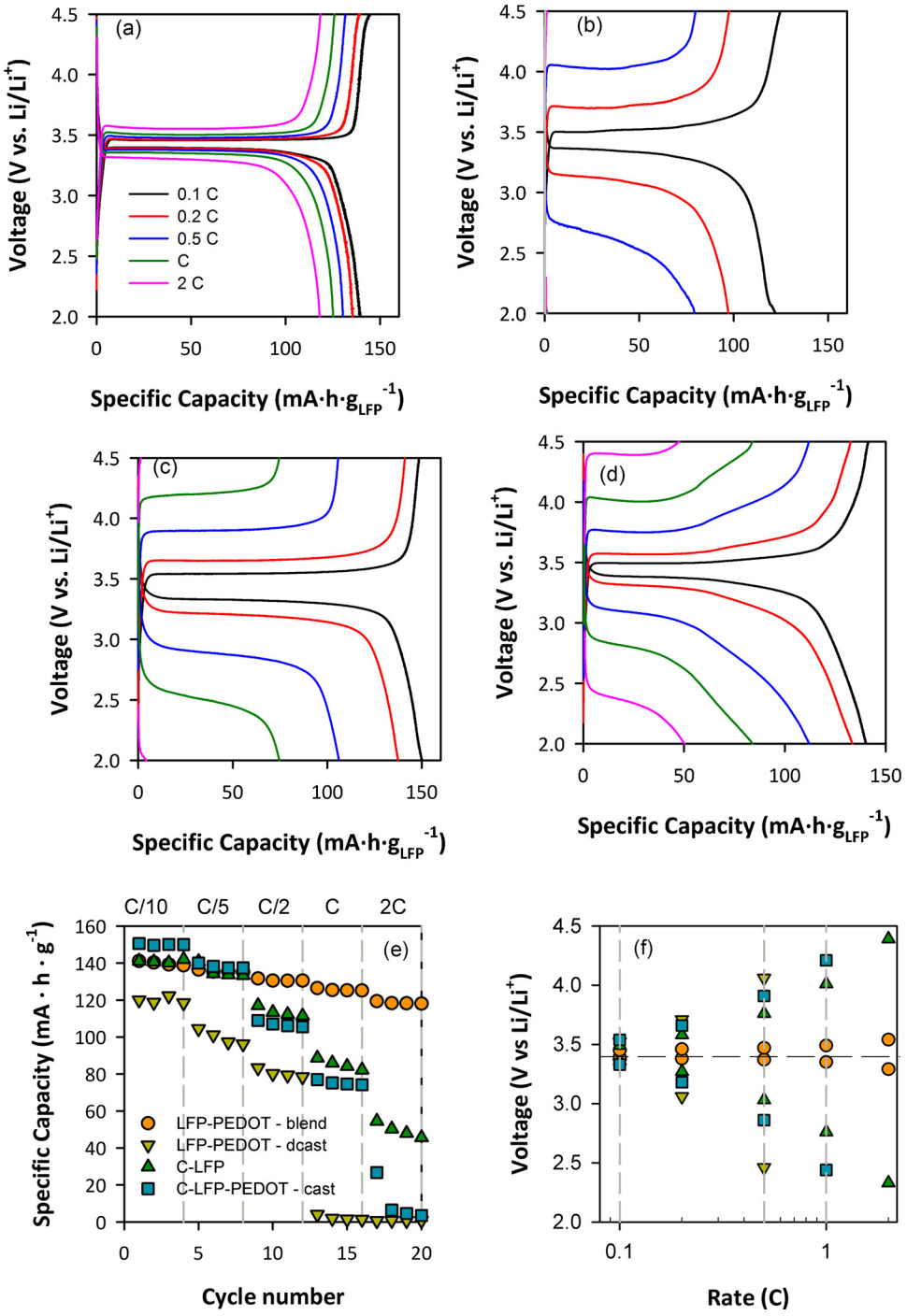

Fig. 3. Charge–Discharge curves (third cycle) at different rates for: a) LFP/PEDOT(blend), b) LFP/PEDOT(cast), c) C-LFP/PEDOT(cast), and d) C-LFP. e) Effect of charge rates on the specific charge capacities for the four studied cathodes. f) Voltage of the charge/discharge plateau vs. C-rate.

slow-rate) version of the CV experiment that corresponds to the derivative of the charge–discharge curve as $C_\mu = -dQ/dV$. An additional capacitive element C_{Li+} accounts for the contribution of inserted Li^+ before reaching stable sites within the matrix, i.e. before the phase $LiFePO_4$ is achieved. This capacitance appears at the intermediate-frequency arc of the impedance plots [23,24].

These considerations suggest a simple equivalent circuit (Fig. 5a) which accounts for the high-frequency response by means of R_{ct} and C_{dl} for both cathodes, and in the particular case of C-LPF also by R_C and C_C. The low-frequency part is modeled by a series combination of resistive R_{lr} (lithiation reaction) and capacitive (chemical) C_μ elements in parallel to C_{Li+}. It is noted here that the equivalent circuit of Fig. 5a models the hindrance in the Li^+ final reaction with the host matrix by means of the resistive element R_{lr}. This is a phenomenological representation of a series of kinetic limitation mechanisms that comprises not only ion transport but also reaction losses, and concomitant restructuring. It was discussed by means of potentiostatic intermittent titration tests that both diffusive transport mechanisms and those related to the first-order phase transition influence the reaction kinetics [28].

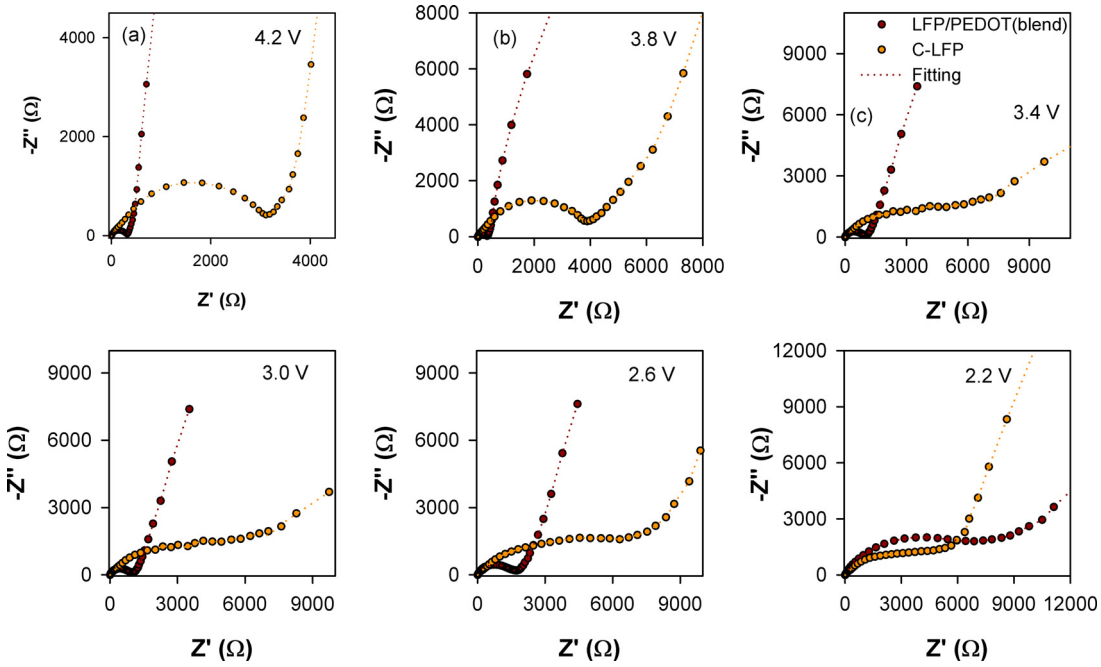

Fig. 4. Nyquist plots of experimentally measured data (circles) and fitting results for the equivalent circuit model (Fig. 5a) at different stages of discharge for: LFP/PEDOT (blend), and C-LFP.

Following related methods allowed determining the true ion diffusion coefficient and the interface mobility of phase transformation electrodes in the two-phase region [29]. Some works concluded that the kinetics of $LiFePO_4$ delithiation is controlled by linear irreversible thermodynamics and found to be characterized by an induction period followed by parabolic growth behavior of the $FePO_4$ phase indicating transport control [30]. Other recent works highlighted that, even for composite electrodes, nucleation and growth govern the electrode kinetics [31] relying on typical chronoamperograms resulting as a consequence of phase transformation. Diffusion impedance simple patterns (Warburg response) are not observed in the experimental data of Fig. 4, in agreement with the absence of Cottrell-like responses in chronoamperograms [31]. Presumably because the electrode structure, formed by a composite with conductive polymers, implies 3D ionic transport [32] in two-phase LFP matrix in the steady state. Therefore the sole impedance analysis cannot allow discarding other kinetic hindrance terms (related to phase transformation) in addition to ion diffusion. As a consequence the resistive element R_{lr} attempts to capture different kinetic limitation contributions without discerning the weight each mechanism has on the overall response. It should be also noted that in comparison with previously proposed equivalent circuits [33], our model connects the low-frequency subcircuit in series with the interfacial charge transfer resistance R_{ct} while putting C_{dl} in parallel. This circuit element connection agrees with the original Randles model accounting for the electrochemical impedance of surfaces.

Main parameters extracted from fitting using the equivalent circuit in Fig. 5a are summarized in Fig. 6. With the calculated values it is easier to understand the lithiation process monitored by impedance spectra (Fig. 4). It is observed that both C-LFP and LFP/PEDOT(blend) electrodes exhibit similar chemical capacitance values (Fig. 6a) peaking at voltages near 3.5 V as the phosphate matrix reacts with Li^+ ions. This agrees with the potential plateau of charging/discharging profiles reported in Fig. 3a and 3d. The observation of similar capacitances informs that the charging ability at sufficiently slow rate (quasi-equilibrium) is comparable

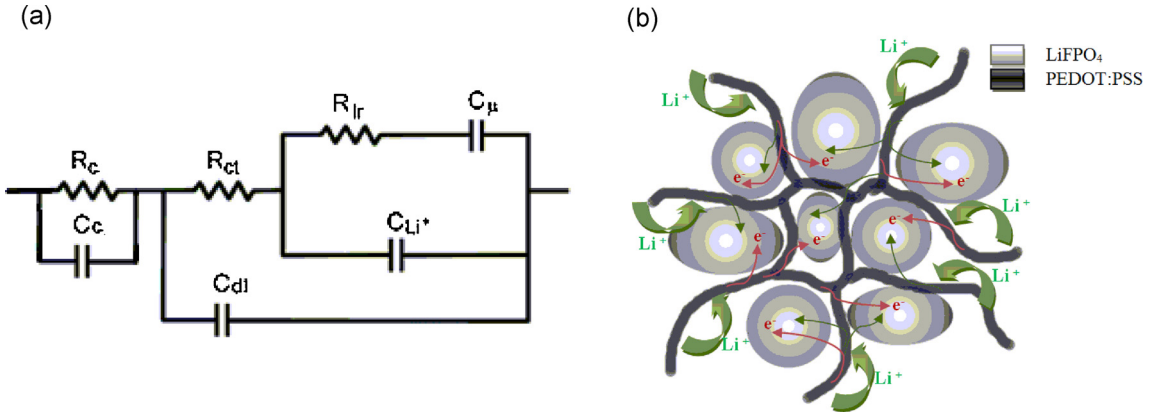

Fig. 5. a) Equivalent circuit used for fitting: i) resistance and capacity ascribed to the C-coating layer, R_c and C_c, for the cathode C-LFP; ii) the interfacial charge-transfer resistance, R_{ct}, combined with the double-layer capacitance, C_{dl}, that dominates the high-frequency response; and iii) reaction subcircuit modeled by chemical capacitance C_μ, Li^+ capacitance C_{Li+}, and lithiation resistance, R_{lr}. b) Scheme of the PEDOT conducting molecular network during lithiation process in LFP/PEDOT(blend) cathode.

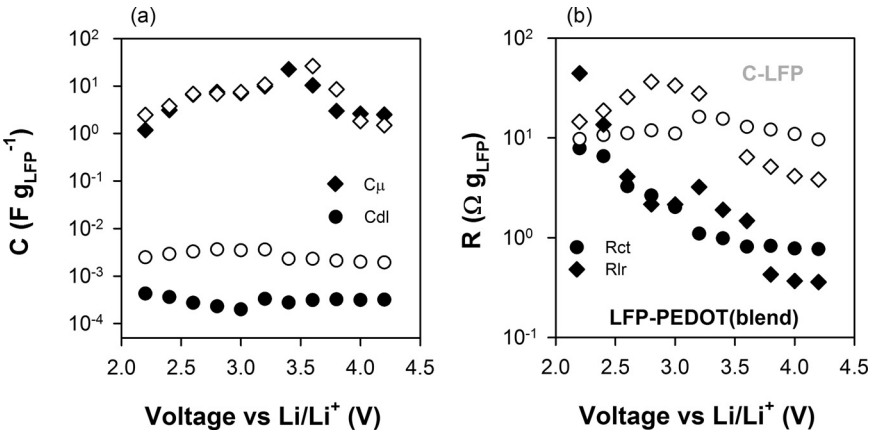

Fig. 6. Fitting parameters in discharge process for LFP/PEDOT(blend) (solid symbols) and C-LFP (hollow symbols): the high frequency response, i.e. transference resistance (R_{ct}) and the double layer capacity (C_{dl}) are symbolized by circles (●), and the low frequency response, i.e. the resistance to the lithiation reaction (R_{lr}) and the chemical capacity (C_{μ}) to rhombus (◆).

and independent on the coating strategy. However, differences in kinetic limitation are evident by examining Fig. 6b. It was found that C-LFP electrodes exhibit higher resistances than LFP/PEDOT (blend) electrodes. In both cases the higher resistance at potentials in excess of 3.9 V is the charge transfer that is one order of magnitude higher for C-LFP than for LFP/PEDOT(blend). In the particular case of C-LFP, R_{lr} increases one order of magnitude and becomes the dominant resistance of the cathode at voltages below 3.5 V. This high resistive value slows down the phosphate lithiation. R_{lr} decreases with further discharge but it maintains high values, ca. 35 Ω g. This explains the wider cathodic peak observed in the CV (Fig. 2) for C-LFP cathode. In the case of LFP/PEDOT(blend), the behavior is different. In this case, R_{lr} at 3.4 V is 3.4 Ω g, at the C_{μ} maximum. The low value of R_{lr} allows a fast lithiation process that is reflected in a well-defined cathodic peak in CV (Fig. 2). As commented previously, the performance at quasi-equilibrium state of the impedance spectra shows that both cathodes have practically the same C_{μ} in all the voltage range, independently of the higher resistances present in the C-LFP cathode, and C_{dl} is higher in this cathode than the registered for LFP/PEDOT(blend). The same discussion can be applied to the charge process, which is performed in SI. Finally, R_c observed for the C-coated LFP particles is constant within the potential range with a value of 0.5 Ω g, that is lower than the other two resistances registered in the system.

These results demonstrate that C-coating and PEDOT(blend) not only facilitate the charge transfer but also influence the resistance of the lithiation of the phosphate matrix. In this aspect, PEDOT(blend) is a more effective strategy, and the resistances in the electrode are below 10 Ω g until high level of lithiation of the cathode. This is caused by the high conductivity of both electrons and ions of the PEDOT polymer [34] and the good embedded structure of the LFP nanoparticles in the PEDOT matrix (Fig. 1b). A scheme of the LFP-PEDOT-blend operation mechanisms is represented in Fig. 5b.

4. Conclusions

The electrochemical effect of the addition to LFP particles of carbon or PEDOT, two of the widely used strategies to increase the conductivity of the $LiFePO_4/FePO_4$ matrix, has been evaluated in terms of resistances and capacities of the different steps in the lithiation/delithiation process present in the cathode. For this purpose, impedance spectra have been registered within the potential range of interest. The Nyquist plots exhibit two patterns with distinguishable time constants associated to specific electrochemical mechanisms. This effect allows to propose an equivalent model in which the high frequency processes are ascribed to surface processes (charge transfer resistance, R_{ct}, and double layer capacity, C_{dl}), and the low frequency response to the lithiation/delithiation inside the phosphate matrix (resistance to the lithiation R_{lr}, and chemical capacity C_{μ}). These results show that both strategies reduce the resistances R_{ct} and R_{lr}, albeit PEDOT is more effective and it is able to reduce the resistances by one order of magnitude compared with C-coating. Suggesting the superior behavior of PEDOT, which favors the kinetics of the lithiation/delithiation processes in the cathode to a large extent. In contrast, both strategies deliver similar thermodynamic properties and show similar chemical capacitances. These results explain that the specific capacity of both cathodes (LFP/PEDOT(blend) and C-LFP) are the same at low charge/discharge current (C/10 and C/5) and close to the theoretical value. When the charge/discharge current increases the LFP/PEDOT(blend) maintains almost complete the specific capacity (130 mA h g_{LFP}^{-1} at 2 C) while for C-LFP the specific capacity decreases notably because of severe resistive limitations.

Acknowledgments

We thank financial support from Generalitat Valenciana (Spain) under project num. ISIC/2012/008 (Institute of Nanotechnologies for Clean Energies), and MEC (Spain) under project num. MAT2011-22753.

Appendix A. Supplementary data

Supplementary data associated with this article can be found, in the online version, at http://dx.doi.org/10.1016/j.electacta.2015.02.148.

References

[1] G.R. Dahlin, K.E. Strøm, Lithium Batteries: Research, Technology, and Applications, Nova Science Publishers, 2010.
[2] B. Kang, G. Ceder, Battery materials for ultrafast charging and discharging, Nature 458 (2009) 190–193.
[3] B. Dunn, H. Kamath, J.-M. Tarascon, Electrical energy storage for the grid: a battery of choices, Science 334 (2011) 928–935.
[4] C. Delmas, M. Maccario, L. Croguennec, F. Le Cras, F. Weill, Lithium deintercalation in $LiFePO_4$ nanoparticles via a domino-cascade model, Nature materials 7 (2008) 665–671.

[5] W. Dreyer, J. Jamnik, C. Guhlke, R. Huth, J. Moškon, M. Gaberšček, The thermodynamic origin of hysteresis in insertion batteries, Nature Materials 9 (2010) 448–453.
[6] D. Xu, X. Chu, Y.-B. He, Z. Ding, B. Li, W. Han, H. Du, F. Kang, Enhanced performance of interconnected $LiFePO_4$/C microspheres with excellent multiple conductive network and subtle mesoporous structure, Electrochimica Acta 152 (2015) 398–407.
[7] Y. Wang, Y. Wang, E. Hosono, K. Wang, H. Zhou, The design of a $LiFePO_4$/carbon nanocomposite with a core–shell structure and its synthesis by an in situ polymerization restriction method, Angewandte Chemie 120 (2008) 7571–7575.
[8] X.L. Wu, L.Y. Jiang, F.F. Cao, Y.G. Guo, L.J. Wan, $LiFePO_4$ Nanoparticles Embedded in a Nanoporous Carbon Matrix: Superior Cathode Material for Electrochemical Energy-Storage Devices, Advanced Materials 21 (2009) 2710–2714.
[9] S.W. Oh, S.T. Myung, S.M. Oh, K.H. Oh, K. Amine, B. Scrosati, Y.K. Sun, Double carbon coating of $LiFePO_4$ as high rate electrode for rechargeable lithium batteries, Advanced Materials 22 (2010) 4842–4845.
[10] Y. Xing, Y.-B. He, B. Li, X. Chu, H. Chen, J. Ma, H. Du, F. Kang, $LiFePO_4$/C composite with 3D carbon conductive network for rechargeable lithium ion batteries, Electrochimica Acta 109 (2013) 512–518.
[11] H.C. Dinh, S.I. Mho, I.H. Yeo, Electrochemical Analysis of Conductive Polymer-Coated $LiFePO_4$ Nanocrystalline Cathodes with Controlled Morphology, Electroanalysis 23 (2011) 2079–2086.
[12] N. Trinh, M. Saulnier, D. Lepage, S. Schougaard, Conductive polymer film supporting $LiFePO_4$ as composite cathode for lithium ion batteries, Journal of Power Sources 221 (2013) 284–289.
[13] D. Cíntora-Juárez, C.P. Vicente, S. Ahmad, J.L. Tirado, Improving the cycling performance of $LiFePO_4$ cathode material by poly (3,4-ethylenedioxythiopene) coating, RSC Advances (2014) .
[14] V. Cauda, D. Pugliese, N. Garino, A. Sacco, S. Bianco, F. Bella, A. Lamberti, C. Gerbaldi, Multi-functional energy conversion and storage electrodes using flower-like Zinc oxide nanostructures, Energy 65 (2014) 639–646.
[15] L. Groenendaal, F. Jonas, D. Freitag, H. Pielartzik, J.R. Reynolds, Poly(3,4-ethylenedioxythiophene) and its derivatives: past, present, and future, Advanced Materials (2000) 481–494.
[16] A.K. Padhi, K. Nanjundaswamy, J.B.D. Goodenough, Phospho-olivines as positive-electrode materials for rechargeable lithium batteries, Journal of the Electrochemical Society 144 (1997) 1188–1194.
[17] M. Armand, M. Gauthier, J.F. Magnan, N. Ravet, New process for synthesizing $limpo_4$ materials with olivine structure, Google Patents, 2002.
[18] C.W. Kim, J.S. Park, K.S. Lee, Effect of Fe_2P on the electron conductivity and electrochemical performance of $LiFePO_4$ synthesized by mechanical alloying using Fe^{3+} raw material, Journal of Power Sources 163 (2006) 144–150.
[19] J.Y. Kim, S.H. Kim, H.H. Lee, K. Lee, W. Ma, X. Gong, A.J. Heeger, New Architecture for High-Efficiency Polymer Photovoltaic Cells Using Solution-Based Titanium Oxide as an Optical Spacer, Advanced Materials (Weinheim, Germany) 18 (2006) 572–576.
[20] N. Recham, L. Dupont, M. Courty, K. Djellab, D. Larcher, M. Armand, J.-M. Tarascon, Ionothermal synthesis of tailor-made $LiFePO_4$ powders for Li-ion battery applications, Chemistry of Materials 21 (2009) 1096–1107.
[21] K.-F. Hsu, S.-Y. Tsay, B.-J. Hwang, Synthesis and characterization of nano-sized $LiFePO_4$ cathode materials prepared by a citric acid-based sol–gel route, Journal of Materials Chemistry 14 (2004) 2690–2695.
[22] G. Arnold, J. Garche, R. Hemmer, S. Ströbele, C. Vogler, M. Wohlfahrt-Mehrens, Fine-particle lithium iron phosphate $LiFePO_4$ synthesized by a new low-cost aqueous precipitation technique, Journal of Power Sources 119 (2003) 247–251.
[23] F. Martinez-Julian, A. Guerrero, M. Haro, J. Bisquert, D. Bresser, E. Paillard, S. Passerini, G. Garcia-Belmonte, Probing Lithiation Kinetics of Carbon-Coated $ZnFe_2O_4$ Nanoparticle Battery Anodes, The Journal of Physical Chemistry C 118 (2014) 6069–6076.
[24] M. Haro, T. Song, A. Guerrero, L. Bertoluzzi, J. Bisquert, U. Paik, G. Garcia-Belmonte, Germanium coating boosts lithium uptake in Si nanotube battery anodes, Physical Chemistry Chemical Physics 16 (2014) 17930–17935.
[25] B. León, C.P. Vicente, J. Tirado, P. Biensan, C. Tessier, Optimized chemical stability and electrochemical performance of $LiFePO_4$ composite materials obtained by ZnO coating, Journal of the Electrochemical Society 155 (2008) A211–A216.
[26] V. Srinivasan, J. Newman, Existence of path-dependence in the $LiFePO_4$ electrode, Electrochemical and solid-state letters 9 (2006) A110–A114.
[27] J. Bisquert, Chemical capacitance of nanostructured semiconductors: its origin and significance for nanocomposite solar cells, Physical Chemistry Chemical Physics 5 (2003) 5360–5364.
[28] N. Meethong, Y.-H. Kao, W.C. Carter, Y.-M. Chiang, Comparative Study of Lithium Transport Kinetics in Olivine Cathodes for Li-ion Batteries, Chemistry of Materials (2010) 1088–1097.
[29] Y. Zhu, C. Wang, Galvanostatic Intermittent Titration Technique for Phase-Transformation Electrodes, J. Phys. Chem. C 114 (2010) 2830–2841.
[30] K. Weichert, W. Sigle, P.A. van Aken, J. Jamnik, C. Zhu, R. Amin, T. Acartürk, U. Starke, J. Maier, Phase Boundary Propagation in Large $LiFePO_4$ Single Crystals on Delithiation, J. Am. Chem. Soc. 134 (2012) 2988–2992.
[31] G. Oyama, Y. Yamada, R.I. Natsui, S.I. Nishimura, A. Yamada, Kinetics of Nucleation and Growth in Two-Phase Electrochemical Reaction of Li_xFePO_4, J. Phys. Chem. C 116 (2012) 7306–7311.
[32] J. Song, M.Z. Bazant, Effects of Nanoparticle Geometry and Size Distribution on Diffusion Impedance of Battery Electrodes, Journal of The Electrochemical Society 160 (2013) A15–A24.
[33] J.P. Schmidt, T. Chrobak, M. Ender, J. Illig, D. Klotz, E. Ivers-Tiffée, Studies on $LiFePO_4$ as cathode material using impedance spectroscopy, Journal of Power Sources 196 (2011) 5342–5348.
[34] G. Li, P.G. Pickup, Ion transport in poly (3,4-ethylenedioxythiophene)–poly (styrene-4-sulfonate) composites, Physical Chemistry Chemical Physics 2 (2000) 1255–1260.